Revision 1

# P-V-T relations of γ-$Ca_3(PO_4)_2$ tuite determined by in situ X-ray diffraction in a large-volume high-pressure apparatus

Shuangmeng Zhai[1], Daisuke Yamazaki[2], Weihong Xue[1], Lijin Ye[1], Chaowen Xu[1], Shuangming Shan[3], Eiji Ito[2], Akira Yoneda[2], Takashi Yoshino[2], Xinzhuan Guo[2], Akira Shimojuku[2], Noriyoshi Tsujino[2], and Ken-Ichi Funakoshi[4]

[1]Key Laboratory of Orogenic Belts and Crustal Evolution, MOE, School of Earth and Space Sciences, Peking University, Beijing 100871, China

[2]Institute for Study of the Earth's Interior, Okayama University, Misasa, Tottori 682-0193, Japan

[3]Institute of Geochemistry, Chinese Academy of Sciences, Guiyang, Guizhou 550002, China

[4]Japan Synchrotron Radiation Research Institute, Sayo, Hyogo 679-5198, Japan

## ABSTRACT

Tuite, γ-$Ca_3(PO_4)_2$, is regarded as an important phosphate mineral in the deep mantle as a host for rare earth elements and large ion lithophile elements, and also for phosphorus. The thermoelastic properties of synthetic γ-$Ca_3(PO_4)_2$ have been determined at simultaneously high pressures and temperatures of up to 35.4 GPa and 1300 K, respectively, by means of in situ energy-dispersive X-ray diffraction measurements in a large-volume multi-anvil apparatus. The pressure-volume-

temperature data obtained for γ-$Ca_3(PO_4)_2$ was fitted by the high-temperature Birch-Murnaghan equation of state to yield $V_0$ = 447.4(4) Å$^3$, $K_{T0}$ = 100.8(18) GPa, $K'_{T0}$ = 5.74(13), $(\partial K_T / \partial T)_P$ = -0.020(1) GPa K$^{-1}$, and $\alpha_T$ = 3.26(18)×10$^{-5}$ + 1.76(24)×10$^{-8}$ $T$. In addition, fitting the present data to the Mie-Grüneisen-Debye equation of state gives $\gamma_0$ = 1.35(6), $\Theta_0$ = 944(136) K, and $q$ = 0.37(29). Based on the thermoelastic properties obtained in the present study, the density profiles of γ-$Ca_3(PO_4)_2$ tuite along typical cold and hot slab geotherms were calculated and were compared with those of the coexisting silicate minerals in subducting mid-ocean ridge basalt.

**Keywords:** γ-$Ca_3(PO_4)_2$ tuite, in situ X-ray diffraction, thermal equation of state, thermoelastic properties

## INTRODUCTION

Tricalcium phosphate is an important compound with at least four polymorphs, including α′-, α-, β-, and γ-$Ca_3(PO_4)_2$. The first three phases are stable from high to low temperature (Fix et al. 1969), while γ-$Ca_3(PO_4)_2$ was first synthesized from β-$Ca_3(PO_4)_2$ at 4 GPa and 950˚C by Roux et al. (1978). This high-pressure polymorph was later found in the decomposed products of hydroxyapatite and fluorapatite at approximately 12 GPa and 1500 K, and was labeled γ-$Ca_3(PO_4)_2$ (Murayama et al. 1986). A naturally occurring γ-$Ca_3(PO_4)_2$ was discovered in a shocked vein of Suizhou L6 chondrite, coexisting with ringwoodite, majorite and hollandite, and was named tuite, and the pressure and temperature conditions for the formation of tuite were

found to be up to 23 GPa and 2000°C, respectively (Xie et al. 2003). It is believed that tuite is a high-pressure polymorph of whitlockite, which is structurally identical to β-$Ca_3(PO_4)_2$ (Xie et al. 2001, 2002). Because of its crystal structure, γ-$Ca_3(PO_4)_2$ was regarded as an important potential host for rare earth elements (REE) and for large ion lithophile elements, such as Sr and Ba, under the pressure and temperature conditions of the upper mantle (Murayama et al. 1986; Sugiyama and Tokonami 1987; Xie et al. 2003). Recently, we synthesized trace element-bearing tuite under high-pressure and high-temperature conditions by using a natural apatite sample as the starting material, and found that the REE concentrations in tuite are two to three orders higher than those in the upper mantle silicate minerals, such as garnet and diopside (Zhai et al. unpublished data).

Apatite is well known as a common accessory mineral in various types of crustal rock, including sedimentary, igneous, and metamorphic rocks (Nash 1984). It is also the most abundant rock-forming phosphate group (McConnell 1973) and is consequently the main phosphorus host in crustal rocks. Apatite may be carried into the mantle by subducting slabs. Therefore, tuite, as one of the decomposed products of apatite, is an important phosphate with significant implications for the geochemistry and mineralogy of the deep mantle. Recently, two experimental studies of apatite-mid-ocean ridge basalt (MORB) and apatite-peridotite systems performed at up to 15 GPa and 19 GPa, respectively, suggested that tuite appears at around 8 GPa in these systems as a phosphate mineral in the upper mantle, and coexists with some silicate minerals, such as garnet and clinopyroxene (Konzett and Frost 2009; Konzett

et al. 2012).

The physical properties of tuite are fundamental for a better understanding of this mineral. In previous studies, some of the physical properties of tuite were investigated by means of X-ray diffraction and Raman spectroscopy at high pressures and temperatures (Zhai et al. 2009; 2010; 2011a), respectively. However, the thermoelastic properties of tuite under simultaneous high-pressure and high-temperature conditions have not yet been examined.

In this study, we investigate the pressure-volume-temperature (*P-V-T*) relations of tuite by in situ energy-dispersive X-ray diffraction measurements using a large-volume high-pressure apparatus combined with synchrotron radiation at the BL04B1 beamline of SPring-8, Japan. The experimental pressure and temperature conditions are up to 24.8 GPa and 1300 K by using tungsten carbide (WC) anvils, and up to 35.4 GPa and 1300 K by using sintered diamond (SD) anvils as the second stage anvils in the Kawai cell, respectively. The high-temperature Birch-Murnaghan (HTBM) equation of state (EoS) and the Mie-Grüneisen-Debye (MGD) EoS were used to fit the *P-V-T* data of tuite to obtain the thermoelastic parameters. Based on these results, the density profiles of tuite were calculated along typical cold and hot slab geotherms and were compared with the coexisting silicate minerals in subducting MORB.

## EXPERIMENTAL DETAILS

Tuite, $\gamma$-$Ca_3(PO_4)_2$, was synthesized under high pressure and temperature

conditions using β-$Ca_3(PO_4)_2$ prepared by a solid state reaction from reagent-grade $CaHPO_4$ and $CaCO_3$, as described in our previous studies (Zhai et al. 2009; 2010). A mixture of tuite and 10 wt% Au was prepared for high-pressure and high-temperature in situ X-ray diffraction measurements.

The high-pressure energy dispersive X-ray diffraction experiments were performed using two multianvil high-pressure apparatuses, SPEED-1500 and SPEED-Mk. II, installed at the BL04B1 beamline of SPring-8. The details of SPEED-1500 and SPEED-Mk. II have been described previously by Utsumi et al. (2002) and Katsura et al. (2004), respectively. We used a Kawai-type cell assembly composed of eight cubic WC and SD anvils for the experiments using SPEED-1500 and SPEED-Mk. II, respectively. The edge lengths of the WC and SD anvils are 26 mm and 14 mm, and the truncated edge lengths of the WC and SD anvils are 2 mm and 1 mm, respectively. The 6.5 mm and 5 mm edge length semi-sintered octahedra made of MgO + 5 wt% $Cr_2O_3$ were used as the pressure media for the WC and SD experiments, respectively. Pyrophyllite was used as the gasket. $TiB_2$ + BN + AlN was used as a tubing heater and sample capsule because of its X-ray transparency. The sample assemblies are shown in Figure 1. In both experiments, the temperature was monitored by the $W_3Re_{97}$-$W_{25}Re_{75}$ thermocouple with its junction centered in the mixture of the sample and the pressure calibrant.

The high-pressure system was combined with a synchrotron radiation source and an energy-dispersive X-ray diffraction system with a Ge solid state detector (SSD) and a charge coupled device camera for the radiographic imaging of the sample. A

polychromatic X-ray beam collimated to dimensions of 0.05 mm horizontally and 0.2 mm vertically was directed at the sample through the pyrophyllite gasket and the pressure medium. A multi-channel analyzer was used to acquire photons in a 20-150 keV range, and was calibrated with the characteristic fluorescence X-ray lines of several reference metals, including Cu, Mo, Ag, Ta, Pt, Au, and Pb. The precision of the energy measurements was approximately 30~100 eV per channel. The 2θ angle of the SSD was set at ~6° with respect to the incident beam direction, and was accurately calibrated using the known diffraction peaks from a standard material, such as Au. The diffraction angle uncertainty after calibration was typically within 0.002°.

Two experiments, S2566 and M990, were carried out by using SPEED-1500 and SPEED-Mk. II, respectively, and the measured P-T paths are shown in Figure 2. In both experiments, the cell assemblies were first compressed to a desired press load at room temperature, and were then heated to 1300 K. Following this, the temperature was first lowered to 1200 K, and then down to 300 K in 150 K steps. For each P-T condition, an X-ray diffraction pattern was collected. The press load was increased after the first data collection cycle, and the temperature was then increased to 1300 K to start another data collection cycle during the cooling process. Several data collection cycles were carried out in the same way. The X-ray diffraction patterns were analyzed using the XRayAnalysis program, which can distinguish and position the peaks precisely. The pressure was determined by using the EoS of Au proposed by Tsuchiya (2003) from the volume calculated using the (111), (200), (220), (311), (222), (400), (331) and (420) diffraction lines. In some cases, one or two diffraction

lines were unavailable to determine the pressure when the Au diffraction peaks overlapped with those of the sample. The uncertainties in the pressure determination were mostly within ± 0.10 GPa. The unit cell parameters of tuite were refined by using the *d* values of the peaks. In run M990, the experiment was terminated because a blow-out occurred while the pressure reached at 39.6 GPa during the cool compression.

## RESULTS AND DISCUSSION

A total of 88 diffraction patterns were collected under various pressure and temperature conditions in the two experiments (see Table 1). Figure 3 shows two representative diffraction patterns collected under high pressure and temperature conditions (Fig. 3a and b) in experiments S2566 and M990, respectively. The X-ray pattern of S2566 under ambient conditions after complete decompression is also shown in Fig. 3c.

### P-V DATA AT ROOM TEMPERATURE

The ambient unit cell parameters of tuite were determined to be $a_0$ = 5.2587(10) Å, $c_0$ = 18.691(4) Å and $V_0$ = 447.6(2) Å$^3$. These values are consistent with those reported in a previous study (Zhai et al. 2009).

The *P-V* data between 0.0 and 39.6 GPa at ambient temperature were fitted using a third-order Birch-Murnaghan (BM) EoS (Birch 1947) in the following form:

$$P = \frac{3}{2} K_0 \left[ \left( \frac{V_0}{V} \right)^{\frac{7}{3}} - \left( \frac{V_0}{V} \right)^{\frac{5}{3}} \right] \times \left\{ 1 - \frac{3}{4} \left( 4 - K_0^{'} \right) \times \left[ \left( \frac{V_0}{V} \right)^{\frac{2}{3}} - 1 \right] \right\}, \quad (1)$$

where $K_0$, $K'_0$, and $V_0$ are the isothermal bulk modulus, its pressure derivation, and the unit-cell volume under ambient conditions, respectively. The results from a least-squares fitting using an EosFit program (Angel 2001) are $V_0$ = 447.4(7) Å$^3$, $K_0$ = 101.6(33) GPa and $K'_0$ = 5.64(25). These values are also consistent with those of our previous study (Zhai et al. 2009). The unit-cell volume data as a function of pressure and the compression curve calculated from the fitted parameters are plotted in Figure 4. When the value of $K'_0$ was set as 4, we then obtained $K_0$ = 124.6(18) GPa, which is higher than the value reported in our previous study (Zhai et al. 2009). Au was actually used as the pressure calibrant in both the present and the previous studies, but a different EoS was used in each case. In the previous study, the EoS for Au proposed by Anderson et al. (1989) was used, whereas in the present study, the EoS derived by Tsuchiya (2003) was used. In a study of $Sr_3(PO_4)_2$, a different EoS of Au gave a slightly different compressibility value (Zhai et al. 2011b). The pressures in the previous diamond anvil cell (DAC) experiment were re-calculated using the EoS of Au proposed by Tsuchiya (2003), and the data were re-analyzed and yielded $K_0$ = 99.4(13) GPa and $K'_0$ = 6.00(17), and $K_0$ = 117.1(15) GPa if $K'_0$ was set at 4. Slight differences remain, which may be attributed to the larger differential stress in the previous DAC experiment compared with that in this study.

## P-V-T RELATIONS AND THERMOELASTIC PARAMETERS

The P-V-T relation of tuite was examined at pressures and temperatures of up to 35.4 GPa and 1300 K using the HTBM EoS proposed by Saxena and Zhang (1990) with the following form:

$$P(V,T) = \frac{3}{2}K_T\left[\left(\frac{V_T}{V}\right)^{\frac{7}{3}} - \left(\frac{V_T}{V}\right)^{\frac{5}{3}}\right]\times\left\{1-\frac{3}{4}\left(4-K_T^{'}\right)\times\left[\left(\frac{V_T}{V}\right)^{\frac{2}{3}}-1\right]\right\}, \quad (2)$$

where $K_T$, $K'_T$, and $V_T$ are the isothermal bulk modulus, its pressure derivation, and the unit-cell volume at temperature $T$ and ambient pressure, respectively, while $V$ is the unit-cell volume at $P$ and $T$. In Equation 2, the bulk modulus pressure derivative ($K'_T$) is assumed to be constant with temperature, and therefore $K'_T = K'_0$. The thermal dependence of the bulk modulus is expressed by a linear function of temperature (Eq. 3), assuming that the temperature derivative is constant over the temperature range of the present study:

$$K_T = K_0 + \left(\frac{\partial K_T}{\partial T}\right)_P (T-300). \quad (3)$$

The temperature derivative of the unit-cell volume $V_T$ can be estimated by a function of the thermal expansion at ambient pressure $\alpha_T$, which is an empirical assumption: $\alpha_T = a_1 + a_2 T$, where $a_1$ and $a_2$ are constant parameters, and

$$V_T = V_0 \exp\int_{300}^{T}\alpha_T dT\,. \quad (4)$$

A least-squares fitting of our data to the HTBM EoS yielded all six parameters ($V_0$, $K_0$, $K'_0$, $(\partial K_T/\partial T)_P$, $a_1$ and $a_2$) simultaneously. The thermoelastic properties of tuite obtained are listed in Table 2, along with the values of the root-mean-square (RMS) misfit in pressure. The results obtained from the HTBM EoS are consistent

with those determined from fitting at room temperature. The *P*-*V*-*T* data obtained and the calculated isothermal compression curves at different temperatures are shown in Figure 5. The observed data are reproduced well by the HTBM EoS.

Figure 6 shows the variations of the isothermal bulk modulus $K_T$ of tuite with temperature. The symbols show the calculated isothermal bulk moduli obtained by fitting the data at each temperature to a third-order BM EoS. The solid squares represent the results of fixing $K'_T$ at 5.74, and the open circles are the results without a fixed value of $K'_T$. The line represents the fit to the HTBM EoS for all of the data as expressed by Equation 3 when using the corresponding parameters listed in Table 2.

The results for tuite show anisotropic elasticity along the *c*-axis and the *a*-axis with increasing pressure and temperature, as illustrated in Figure 7. The ratios of *c/a* generally increase with increasing pressure, which is consistent with the results of our previous DAC experiment at room temperature (Zhai et al. 2009). The ratios of *c/a* decrease with increasing temperature. This means that the *a*-axis is more compressible under pressure and more thermally expansible when compared with the *c*-axis. It appears that the temperature dependence of the ratios of *c/a* differs with varying pressure. Under low pressure, the ratios of *c/a* show slight temperature dependence, while at high pressure, the ratios of *c/a* show major temperature dependence. The effect of the pressure on the temperature dependence of the ratios of *c/a* increases with increasing pressure. The crystal structure of tuite may remain stable at higher pressures and temperatures, which indicates that tuite is likely to be stable over a wide *P*-*T* range in the deep mantle.

The *P-V-T* data of the present study has also been fitted by adopting the MGD EoS (c.f. Jackson and Rigden 1996). In this model, the pressure is described by the sum of the static pressure at room temperature and the thermal pressure, as given by the following equations:

$$P(V,T) = P(V,T_0) + \Delta P_{th}(V,T), \quad (5)$$

$$\Delta P_{th}(V,T) = \frac{\gamma(V)}{V}\left[E_{th}(V,T) - E_{th}(V,T_0)\right], \quad (6)$$

where the static pressure $P(V,T_0)$ is described as a third-order BM EoS, as in Equation 1, whereas the thermal pressure $\Delta P_{th}(V,T)$ is expressed as a function of the Grüneisen parameter $\gamma$ and the thermal energy $E_{th}(V,T)$ with the following expressions:

$$E_{th}(V,T) = \frac{9nRT}{(\Theta/T)^3}\int_0^{\Theta/T}\frac{x^3}{e^x - 1}dx, \quad (7)$$

$$\Theta = \Theta_0 \exp(\frac{\gamma_0 - \gamma}{q}), \quad (8)$$

$$\gamma = \gamma_0 (\frac{V}{V_0})^q, \quad (9)$$

where $n$ is the number of atoms per formula unit, $R$ is the gas constant, $\Theta_0$ is the Debye temperature at ambient pressure, $\Theta$ is the Debye temperature as a function of volume, $\gamma_0$ is the Grüneisen parameter at ambient pressure, and $q$ is the volume dependence of the Grüneisen parameter $\gamma$.

Six parameters ($V_0$, $K_0$, $K'_0$, $\gamma_0$, $\Theta_0$ and $q$) can be obtained by fitting our *P-V-T* data to the MGD EoS, giving values of 447.3(4) Å$^3$, 101.8(19) GPa, 5.64(14), 1.35(6), 944(136) K, and 0.37(29), respectively. Fittings by using both HTBM and MGD EoSs give consistent results for $V_0$, $K_0$, and $K'_0$.

## DENSITY OF TUITE IN SUBDUCTED SLABS

As mentioned above, tuite is regarded as an important phosphate with implications for geochemistry and mineralogy in the deep mantle. In the apatite-MORB and apatite-peridotite systems, tuite appears at around 8 GPa and 1000 °C, coexisting with some mantle silicate minerals, including garnet, clinopyroxene, and stishovite (Konzett and Frost 2009; Konzett et al. 2012). Using the thermoelastic parameters of tuite obtained by fitting to the HTBM EoS in this study, we can calculate the density of tuite in subducting slabs along typical cold and hot geotherms (Thompson 1992), as shown in Figure 8. In the upper mantle, the density of tuite in a cold slab is about 1% higher than that in a hot slab, and this difference decreases with increasing subducting depth. The density profiles of stishovite, garnet, clinopyroxene, and their sequent phases were also calculated for comparison, based on their thermoelastic parameters along a cold slab geotherm (Thompson 1992). The data sources used were: Nishihara et al. (2005) for stishovite (St) with $\rho_0$ = 4.286 g/cm$^3$; Wang et al. (1998) for majoritic garnet (Gt) with $\rho_0$ = 3.71 g/cm$^3$ (Ono et al. 2001); Nishihara et al. (2003) for clinopyroxene (Cpx) with $\rho_0$ = 3.26 g/cm$^3$; Wang et al. (1996) for Ca-perovskite (Ca-Pv) with $\rho_0$ = 4.23 g/cm$^3$; and Funamori et al. (1996) for Mg-perovskite (Mg-Pv) with $\rho_0$ = 4.41 g/cm$^3$ (Ono et al. 2001).

Compared with the coexisting silicate minerals in the apatite-MORB system along a cold subducting slab, the density of tuite is higher than that of clinopyroxene but lower than the densities of the other silicate minerals. After clinopyroxene

disappears, tuite has the lowest density in the deep mantle. Therefore, the buoyancy increases with increasing amounts of tuite in the subducting MORB. However, the amount of tuite is quite small when compared with the major silicate mineral phases in the subducting MORB, which makes it difficult to draw a quantitative conclusion on the buoyancy effect.

## ACKNOWLEDGMENTS

The synchrotron radiation experiments were carried out at the BL04B1 beamline, SPring-8, Japan (Proposal Nos. 2011A1072 and 2012A1139). The authors would like to thank J. Kung, R. Miletich and an anonymous reviewer for their helpful comments and suggestions. This work was financially supported by the NSFC (Grant Nos. 40973045 and 41202020) and partially supported by the Visiting Researcher's Program of the Institute for Study of the Earth's Interior, Okayama University.

## REFERENCES CITED

Anderson, O.L., Isaak, D.G., and Yamamoto, S. (1989) Anharmonicity and the equation of state for gold. Journal of Applied Physics, 65, 1534-1543.

Angel, R.J. (2001) Equations of state. Reviews in Mineralogy and Geochemistry, 41, 35-60.

Birch, F. (1947) Finite elastic strain of cubic crystals. Physical Reviews, 71, 809-924.

Fix, W., Heymann, H., Heinke, R. (1969) Subsolidus relations in the system $2CaO{\cdot}SiO_2$-$3CaO{\cdot}P_2O_5$. Journal of the American Ceramic Society, 52:346-347.

Funamori, N., Yagi, T., Utsumi, W., Kondo, T., Uchida, T., and Funamori, M. (1996) Thermoelastic properties of $MgSiO_3$ perovskite determined by in situ X ray observations up to 30 GPa and 2000 K. Journal of Geophysical Research, 101, 8257-8269.

Jackson, I. and Rigden, S.M. (1996) Analysis of *P-V-T* data: constraints on the thermoelastic properties of high-pressure minerals. Physics of the Earth and Planetary Interiors, 96, 85-112.

Katsura, T., Funakoshi, K., Kubo, A., Nishiyama, N., Tange, Y., Sueda, Y., Kubo, T., and Utsumi, W. (2004) A large-volume high-pressure and high-temperature apparatus for *in situ* X-ray observation, '*SPEED-Mk.II*'. Physics of the Earth and Planetary Interiors, 143-144, 497-506.

Konzett, J. and Frost, D.J. (2009) The high *P–T* stability of hydroxyl-apatite in natural and simplified MORB—an experimental study to 15 GPa with implications for transport and storage of phosphorus and halogens in subduction zones. Journal of Petrology, 50, 2043-2062.

Konzett, J., Rhede, D., and Frost, D.J. (2012) The high PT stability of apatite and Cl partitioning between apatite and hydrous potassic phases in peridotite: an experimental study to 19 GPa with implications for the transport of P, Cl and K in the upper mantle. Contributions to Mineralogy and Petrology, 163, 277-296.

McConnell, D. (1973) Apatite: Its Crystal Chemistry, Mineralogy, Utilization and Biologic Occurrences. Springer Verlag, New York.

Murayama, J.K., Nakai, S., Kato, M., and Kumazawa, M. (1986) A dense polymorph

of $Ca_3(PO_4)_2$: a high pressure phase of apatite decomposition and its geochemical significance. Physics of the Earth and Planetary Interiors, 44, 293-303.

Nash, W.P. (1984) Phosphate minerals in terrestrial igneous and metamorphic rocks. In J.O. Nriagu and P.B. Moore, Eds., Phosphate Minerals, pp. 215-241. Springer-Verlag.

Nishihara, Y., Nakayama, K., Takahashi, E., Iguch, T., and Funakoshi, K. (2005) P-V-T equation of state of stishovite to the lower mantle transition zone conditions. Physics and Chemistry of Minerals, 31, 660-670.

Nishihara, Y., Takahashi, E., Matsukage, K., and Kikegawa, T. (2003) Thermal equation of state of omphacite. American Mineralogist, 88, 80-86.

Ono, S., Ito, E., and Katsura, T. (2001) Mineralogy of subducted basaltic crust (MORB) from 25 to 37 GPa, and chemical heterogeneity of the lower mantle. Earth and Planetary Science Letters, 190, 57-63.

Roux, P., Lowor, D., and Bonel, G. (1978) Sur une novella forme cristallite du phosphate tricalcique. Comptes Rendus de l'Académie des Sciences. Série C, 286, 549-551.

Saxena, S. and Zhang, J. (1990) Thermochemical and pressure-volume-temperature systematics of data on solid, exzamples: Tungsten and MgO. Physics and Chemistry of Minerals, 17, 45-51.

Sugiyama, K. and Tokonami, M. (1987) Structure and crystal chemistry of a dense polymorph of tricalcium phosphate $Ca_3(PO_4)_2$: A host to accommodate large lithophile elements in the Earth's mantle. Physics and Chemistry of Minerals, 15,

125-130.

Thompson, A.B. (1992) Water in the Earth's upper mantle. Nature, 358, 295-302.

Tsuchiya, T. (2003) First-principles prediction of the *P-V-T* equation of state of gold and the 660-km discontinuity in Earth's mantle. Journal of Geophysical Research, 108, 2462, doi: 10.1029/2003JB002446.

Utsumi, W., Funakoshi, K., Katayama, Y., Yamakata, M., Okada, T., and Shimomura, O. (2002) High-pressure science with a muli-anvil apparatus at SPring-8. Journal of Physics: Condensed Matter, 14, 10497-10504.

Wang, Y., Weidner, D.J., and Guyot, F. (1996) Thermal equation of state of $CaSiO_3$ perovskite. Journal of Geophysical Research, 101, 661-672.

Wang, Y., Weidner, D.J., Zhang, J., Gwanmesia, G.D., and Liebermann, R.C. (1998) Thermal equation of state of garnets along the pyrope-majorite join. Physics of the Earth and Planetary Interiors, 105, 59-71.

Xie, X., Minitti, M.E., Chen, M., Mao, H.K., Wang, D., Shu, J., Fei, Y. (2001) High-pressure polymorph of $Ca_3(PO_4)_2$ in the shock melt veins of the Suizhou L6 chondrite. Lunar and Planetary Science, 32, 1358.

Xie, X., Minitti, M.E., Chen, M., Mao, H.K., Wang, D., Shu, J., Fei, Y. (2002) Natural high-pressure polymorph of merrillite in the shock vein of the Suizhou meteorite. Geochimica et Cosmochimica Acta, 66, 2439-2444.

Xie, X., Minitti, M.E., Chen, M., Mao, H.K., Wang, D., Shu, J., and Fei, Y. (2003) Tuite, $\gamma$-$Ca_3(PO_4)_2$: a new mineral from the Suizhou L6 chondrite. European Journal of Mineralogy, 15, 1001-1005.

Zhai, S., Liu, X., Shieh, S., Zhang, L., and Ito, E. (2009) Equation of state of γ-tricalcium phosphate, γ-$Ca_3(PO_4)_2$, to lower mantle pressures. American Mineralogist, 94, 1388-1391.

Zhai, S., Wu, X., and Ito, E. (2010) High-pressure Raman spectra of tuite, γ-$Ca_3(PO_4)_2$. Journal of Raman Spectroscopy, 41, 1011-1013.

Zhai, S., Xue, W., Lin, C., Wu, X., and Ito, E. (2011a) Raman spectra and X-ray diffraction of tuite at various temperatures. Physics and Chemistry of Minerals, 38, 639-646.

Zhai, S., Xue, W., Yamazaki, D., Shan, S., Ito, E., Tomioka, N., Shimojuku, A., and Funakoshi, K. (2011b) Compressibility of strontium orthophosphate $Sr_3(PO_4)_2$ at high pressure. Physics and Chemistry of Minerals, 38, 357-361.

358 **Figure Captions**

359 Figure 1. Schematic drawings of the sample assemblies. (a) Cross section of a
360 6.5-2 sample assembly for WC anvils. (b) Cross section of a 5-1 sample assembly for
361 SD anvils.

362

363 Figure 2. P-T paths of the in situ X-ray diffraction experiments. Open circles:
364 S2566; solid triangles: M990.

365

366 Figure 3. Typical X-ray diffraction patterns of tuite obtained in the present study.
367 Abbreviations indexed to the diffraction peaks: *T*: tuite, γ-$Ca_3(PO_4)_2$; *Au*: gold; *:
368 X-ray fluorescence of Au; *M*: MgO from the pressure medium; *TB*: $TiB_2$ heater.

369

370 Figure 4. P-V relation of compression data for tuite at ambient temperature
371 obtained in this study (solid squares), compared with our previous data from the DAC
372 experiment (Zhai et al. 2009) (open squares). The dashed curve represents a
373 third-order Birch-Murnaghan equation fitting with $K_0$ and $K'_0$ values of 101.6 GPa and
374 5.64, respectively. The error bars are smaller than the sizes of the symbols used.

375

376 Figure 5. P-V-T data points for tuite obtained in this study. The error bars are
377 smaller than the size of the symbols used. Isothermal compression curves at various
378 temperatures (dashed lines) represent the HTBM EoS fittings at 300, 450, 600, 750,
379 900, 1050, 1200, and 1300 K, with the following parameters: $V_0$ = 447.4(4) $Å^3$, $K_0$ =

100.8(18) GPa, $K'_0$= 5.74(13), $(\partial K_T / \partial T)_P$ = -0.020(1), $a_1 = 3.26\times10^{-5}$ $K^{-1}$, and $a_2 = 1.76(24)\times10^{-8}$ $K^{-2}$ (RMS misfit = 0.188 GPa).

Figure 6. Variations of the isothermal bulk modulus of tuite against temperature. Open circles denote the isothermal bulk moduli calculated by fitting the data at each temperature, and solid squares denote the isothermal bulk moduli calculated by fitting the data at each temperature with $K'_T$ fixed at 5.74. The solid line represents the fitting to the HTBM EoS (Table 2).

Figure 7. Variation of the *c/a* ratio with pressure and temperature.

Figure 8. Calculated density profiles of tuite along the typical geotherms of cold (thick solid line) and hot (dashed line) slabs (Thompson 1992) as a function of pressure. The density profiles of some coexisting silicate minerals and their sequent phases are also calculated for comparison, based on their thermoelastic parameters along a cold slab geotherm (Thompson 1992). The phase abbreviations are: tuite, Tu; clinopyroxene, Cpx; garnet, Gt; stishovite, St; Mg-perovskite, Mg-Pv; Ca-perovskite, Ca-Pv.

398 Table 1. Pressure, temperature, lattice parameters and unit cell volume of tuite

| *P* (GPa) | *T* (K) | *a* (Å) | *c* (Å) | *V* (Å$^3$) |
|---|---|---|---|---|
| Run S2566 | | | | |
| 0.00(0) | 300 | 5.2587(10) | 18.691(4) | 447.6(2) |
| 4.91(8) | 300 | 5.1785(20) | 18.448(16) | 428.4(4) |
| 7.29(11) | 300 | 5.1467(38) | 18.407(21) | 422.2(6) |
| 5.18(4) | 1300 | 5.2364(24) | 18.701(18) | 444.1(4) |
| 5.02(8) | 1200 | 5.2312(13) | 18.668(9) | 442.4(2) |
| 4.69(8) | 1050 | 5.2248(12) | 18.651(9) | 440.9(2) |
| 4.46(5) | 900 | 5.2191(11) | 18.635(8) | 439.6(2) |
| 4.11(4) | 750 | 5.2137(11) | 18.604(8) | 437.9(2) |
| 3.82(4) | 600 | 5.2071(9) | 18.584(6) | 436.4(1) |
| 3.50(4) | 450 | 5.2018(10) | 18.555(7) | 434.8(2) |
| 3.40(5) | 303 | 5.1949(13) | 18.531(9) | 433.1(2) |
| 8.63(12) | 300 | 5.1238(19) | 18.343(12) | 417.1(3) |
| 9.43(7) | 1300 | 5.1712(12) | 18.501(8) | 428.5(2) |
| 9.17(8) | 1200 | 5.1679(10) | 18.489(6) | 427.6(2) |
| 9.00(7) | 1050 | 5.1622(10) | 18.470(6) | 426.3(2) |
| 8.72(8) | 900 | 5.1562(11) | 18.467(5) | 425.2(2) |
| 8.16(6) | 750 | 5.1514(8) | 18.442(3) | 423.8(1) |
| 7.95(8) | 600 | 5.1458(12) | 18.412(7) | 422.2(2) |
| 7.74(5) | 450 | 5.1398(13) | 18.408(5) | 421.1(2) |

| | | | | |
|---|---|---|---|---|
| 7.55(8) | 304 | 5.1357(9) | 18.378(6) | 419.8(1) |
| 10.74(9) | 300 | 5.1000(15) | 18.282(9) | 411.8(2) |
| 14.52(5) | 300 | 5.0621(16) | 18.181(10) | 403.5(2) |
| 15.85(9) | 1300 | 5.0879(13) | 18.284(8) | 409.9(2) |
| 15.68(10) | 1200 | 5.0845(13) | 18.275(7) | 409.1(2) |
| 15.31(8) | 1050 | 5.0802(14) | 18.263(8) | 408.2(2) |
| 15.05(9) | 900 | 5.0763(13) | 18.246(8) | 407.2(2) |
| 14.89(10) | 750 | 5.0716(15) | 18.239(9) | 406.3(2) |
| 14.32(11) | 600 | 5.0679(14) | 18.224(8) | 405.4(2) |
| 14.25(11) | 450 | 5.0644(15) | 18.213(9) | 404.5(2) |
| 13.95(8) | 304 | 5.0595(10) | 18.205(7) | 403.6(2) |
| 18.67(9) | 300 | 5.0135(14) | 18.093(8) | 393.8(2) |
| 19.81(5) | 1300 | 5.0431(8) | 18.173(3) | 400.3(1) |
| 19.53(7) | 1200 | 5.0400(8) | 18.159(4) | 399.5(10) |
| 19.28(7) | 1050 | 5.0358(8) | 18.148(4) | 398.6(1) |
| 19.01(11) | 900 | 5.0311(10) | 18.137(5) | 397.6(1) |
| 18.77(10) | 750 | 5.0271(11) | 18.126(5) | 396.7(1) |
| 18.59(10) | 600 | 5.0225(11) | 18.116(5) | 395.8(1) |
| 18.32(11) | 450 | 5.0177(11) | 18.111(6) | 394.9(1) |
| 18.19(11) | 303 | 5.0164(11) | 18.100(6) | 394.5(1) |
| 22.14(10) | 300 | 4.9808(11) | 18.022(6) | 387.2(2) |
| 22.62(7) | 1300 | 5.0160(9) | 18.094(5) | 394.3(1) |

| | | | | |
|---|---|---|---|---|
| 22.22(8) | 1200 | 5.0166(8) | 18.108(5) | 394.7(1) |
| 22.07(10) | 1050 | 5.0102(11) | 18.087(6) | 393.2(2) |
| 22.02(11) | 900 | 5.0058(12) | 18.077(6) | 392.3(2) |
| 21.66(11) | 750 | 5.0011(12) | 18.072(7) | 391.5(2) |
| 21.05(11) | 600 | 4.9978(10) | 18.060(5) | 390.7(1) |
| 21.29(11) | 450 | 4.9936(13) | 18.049(7) | 389.8(2) |
| 20.86(9) | 305 | 4.9899(11) | 18.046(6) | 389.1(2) |
| 24.43(6) | 300 | 4.9604(13) | 17.960(7) | 382.7(2) |
| 24.81(8) | 1300 | 4.9972(9) | 18.051(6) | 390.4(1) |
| 24.47(8) | 1200 | 4.9950(11) | 18.052(6) | 390.1(1) |
| 24.31(11) | 1050 | 4.9910(8) | 18.040(5) | 389.2(1) |
| 24.02(8) | 900 | 4.9875(9) | 18.034(5) | 388.5(1) |
| 23.75(9) | 750 | 4.9836(7) | 18.020(4) | 387.6 (1) |
| 23.31(9) | 600 | 4.9802(7) | 18.012(4) | 386.9(1) |
| 23.24(9) | 450 | 4.9764(7) | 18.005(4) | 386.1(1) |
| 22.85(9) | 304 | 4.9720(7) | 18.002(5) | 385.4(1) |
| 25.65(10) | 300 | 4.9535(10) | 17.949(6) | 381.1(2) |
| Run M990 | | | | |
| 9.54(10) | 300 | 5.1083(11) | 18.323(4) | 414.1(2) |
| 17.87(12) | 300 | 5.0237(10) | 18.105(4) | 395.7(2) |
| 22.21(13) | 300 | 4.9799(10) | 18.013(4) | 386.9(2) |
| 22.77(9) | 1300 | 5.0222(7) | 18.113(4) | 395.7(1) |

| | | | | |
|---|---|---|---|---|
| 22.63(6) | 1200 | 5.0134(6) | 18.097(3) | 393.9(1) |
| 22.40(5) | 1050 | 5.0122(6) | 18.096(3) | 393.7(1) |
| 22.21(4) | 900 | 5.0079(7) | 18.087(3) | 392.8(1) |
| 21.50(7) | 750 | 5.0042(8) | 18.082(3) | 392.1(1) |
| 20.85(4) | 600 | 5.0007(9) | 18.073(4) | 391.4(1) |
| 20.39(4) | 450 | 4.9976(7) | 18.067(3) | 390.8(1) |
| 20.33(8) | 303 | 4.9938(9) | 18.066(4) | 390.2(1) |
| 26.05(8) | 300 | 4.9500(6) | 17.944(3) | 380.8(1) |
| 26.91(7) | 1300 | 4.9790(7) | 18.013(3) | 386.7(1) |
| 26.83(7) | 1200 | 4.9742(7) | 18.006(3) | 385.8(1) |
| 26.65(4) | 1050 | 4.9699(11) | 18.002(4) | 385.1(2) |
| 26.37(5) | 900 | 4.9667(7) | 17.986(3) | 384.2(1) |
| 25.89(6) | 750 | 4.9635(7) | 17.975(5) | 383.5(1) |
| 25.65(5) | 600 | 4.9607(7) | 17.971(5) | 383.0(1) |
| 25.41(9) | 450 | 4.9564(9) | 17.976(4) | 382.4(1) |
| 25.10(7) | 304 | 4.9538(7) | 17.974(3) | 382.0(1) |
| 35.32(10) | 300 | 4.8773(10) | 17.793(4) | 366.6(1) |
| 35.42(8) | 1300 | 4.9122(6) | 17.846(2) | 372.9(1) |
| 35.62(11) | 1200 | 4.9077(7) | 17.844(3) | 372.2(1) |
| 35.16(8) | 1050 | 4.9045(7) | 17.837(3) | 371.6(1) |
| 34.88(5) | 900 | 4.8997(10) | 17.834(4) | 370.8(1) |
| 34.85(8) | 750 | 4.8979(5) | 17.820(2) | 370.2(1) |

| | | | | |
|---|---|---|---|---|
| 34.21(7) | 600 | 4.8947(6) | 17.822(2) | 369.8(1) |
| 33.68(9) | 450 | 4.8912(6) | 17.824(2) | 369.3(1) |
| 33.27(5) | 304 | 4.8883(7) | 17.825(3) | 368.9(1) |
| 39.59(10) | 300 | 4.8557(6) | 17.725(2) | 361.9(1) |

399 The values in parentheses are the standard deviations and refer to the last digit.

400 Table 2. Thermoelastic parameters of tuite obtained from fittings to HTBM EoS

| | |
|---|---|
| $V_0$ (Å$^3$) | 447.4(4) |
| $K_0$ (GPa) | 100.8(18) |
| $K'_0$ | 5.74(13) |
| $(\partial K_T / \partial T)_P$ (GPa K$^{-1}$) | -0.020(1) |
| $a_1$ ($10^{-5}$ K$^{-1}$) | 3.26(18) |
| $a_2$ ($10^{-8}$ K$^{-2}$) | 1.76(24) |
| $\alpha_{300}$ ($10^{-5}$ K$^{-1}$) | 3.79(19) |
| RMS misfit (GPa) | 0.188 |

401

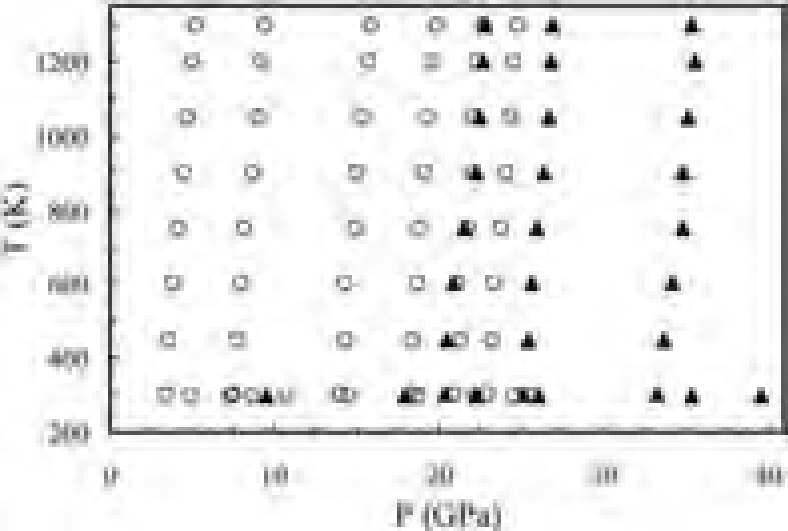
T (K)
P (GPa)

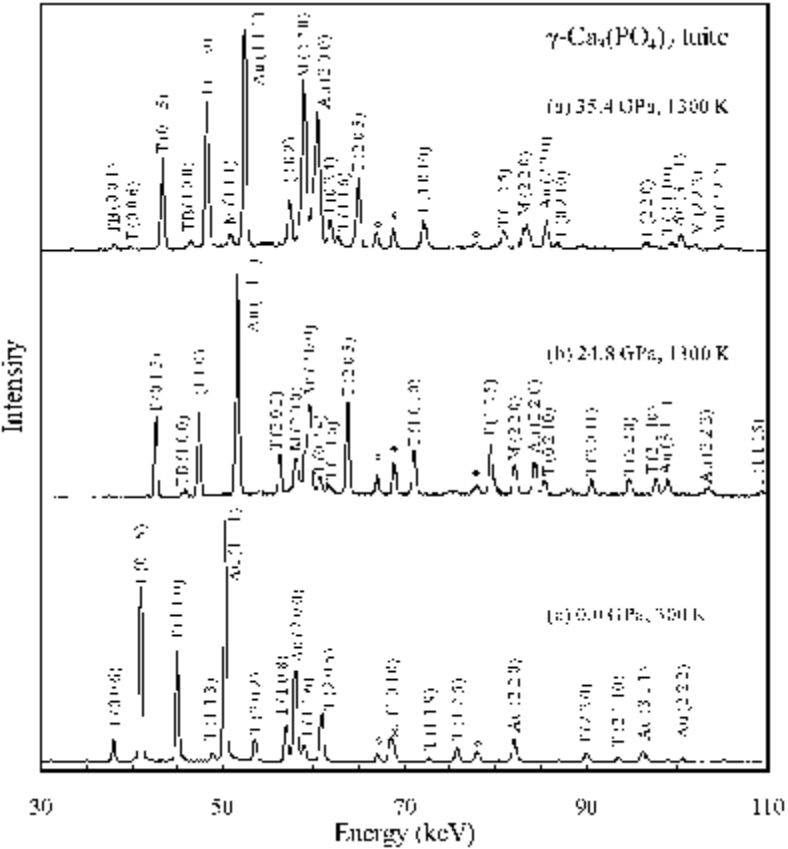
γ-Ca3(PO4)2 brite
(a) 35.4 GPa, 1300 K
(b) 21.8 GPa, 1900 K
(c) 0.0 GPa, 300 K
Intensity
30
50
70
90
110
Energy (keV)

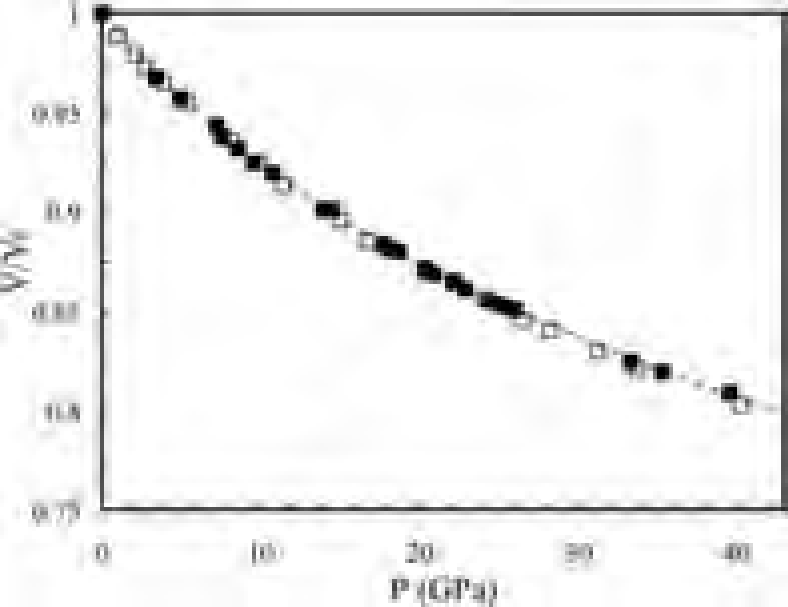
0.95
0.9
0.85
0.8
0.75
V/V
0
10
20
30
40
P (GPa)

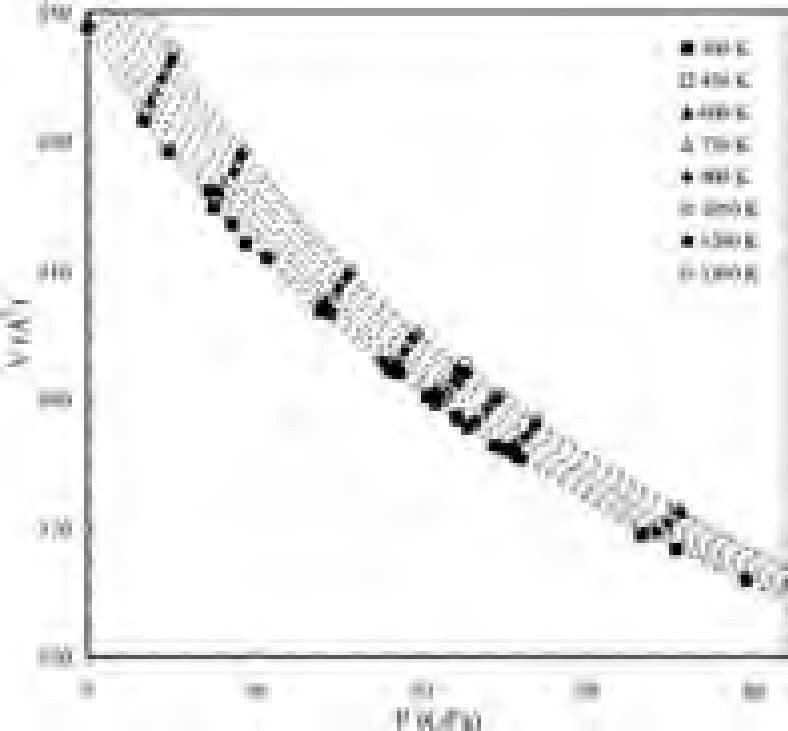

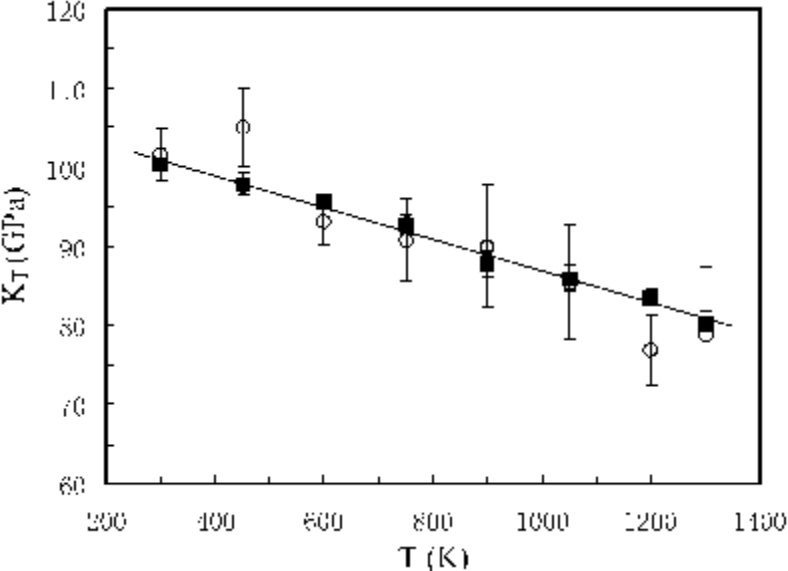
120
110
100
90
80
70
60
$K_T$ (GPa)
200
400
600
800
1000
1200
1400
T (K)

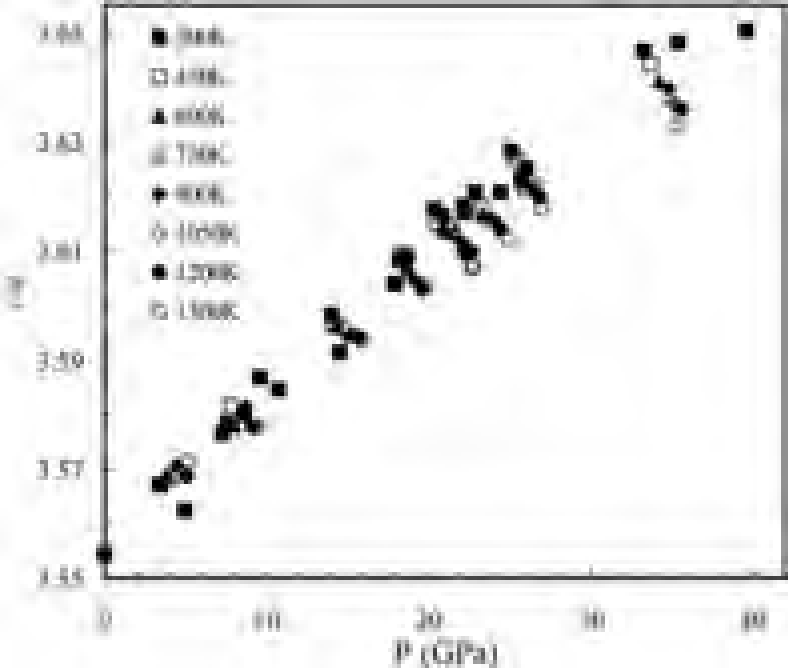
3.65
3.63
3.61
3.59
3.57
3.55
0
10
20
30
40
P (GPa)

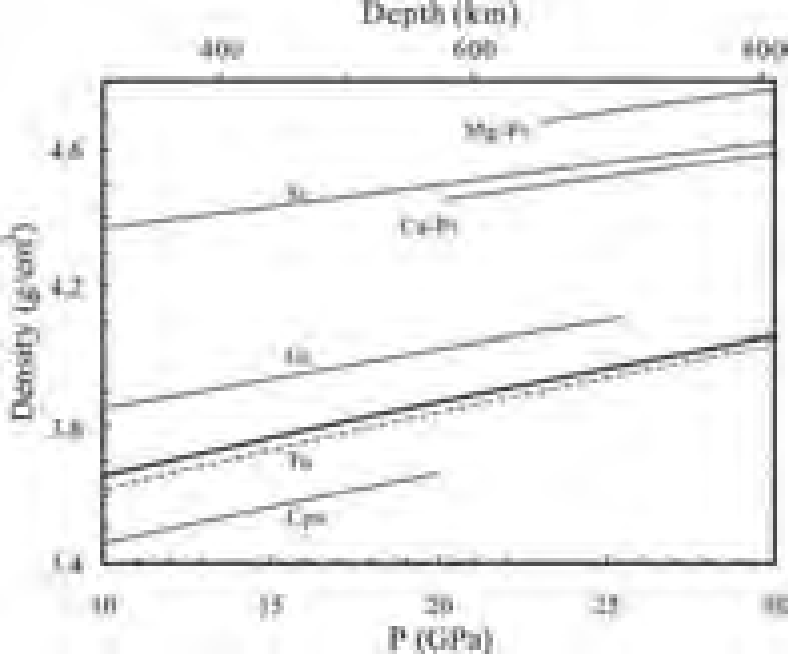
Depth (km)
400
600
Density (g/cm³)
4.6
4.2
3.8
3.4
10
15
20
25
P (GPa)